

Characterizing the QPO Behavior of the X-ray Nova XTE J1550–564

Ronald A. Remillard¹, Gregory J. Sobczak², Michael P. Muno¹, and Jeffrey E. McClintock³

ABSTRACT

For all 209 RXTE observations of the X-ray nova XTE J1550–564 during its major outburst of 1998-1999, we have analyzed the X-ray power spectra, phase lags, and coherence functions. These observations constitute one of the richest and most complete data sets obtained for any black hole X-ray nova. The phase lags and coherence measures are used to distinguish three types of low-frequency QPOs (one more than those reported by Wijnands, Homan, & van der Klis 1999). For the most common type (“C”), the phase lag is correlated with both the QPO frequency and the amplitude. The physical significance of the QPO types is evident in the relationships between QPO properties and the apparent temperature and flux from the accretion disk. There is also a clear pattern in how the QPO types relate to the presence of high-frequency QPOs. In general, both the amplitude and the Q value ($\nu/FWHM$) of low-frequency QPOs decrease as the high-frequency oscillations increase in frequency (100 to 284 Hz) and in Q value. We speculate that the antagonism between low-frequency and high-frequency QPOs arises from competing structures in a perturbed accretion disk. However, we find that the frequencies of slow (< 20 Hz) and fast (> 100 Hz) QPOs are not correlated. In addition, we encounter systematic problems in attempting to reliably compare the QPO frequencies with broad features in the power continuum, since there are a variable number of features or spectral breaks in the power spectra. These results cast some doubt on the reported global relationship between QPOs from neutrons stars and those from black hole systems.

Subject headings: black hole physics — stars: individual (XTE J1550–564) — X-rays: stars

¹Center for Space Research, MIT, Cambridge, MA 02139; rr@space.mit.edu, muno@space.mit.edu

²Harvard University, Astronomy Dept., 60 Garden St. MS-10, Cambridge, MA 02138

³Harvard-Smithsonian Center for Astrophysics, 60 Garden St. MS-3, Cambridge, MA 02138; jem@cfa.harvard.edu

1. Introduction

XTE J1550–564 is an X-ray nova and black hole candidate discovered with the All Sky Monitor (ASM; Levine et al. 1996) on board the *Rossi X-ray Timing Explorer* (RXTE) in 1998 September (Smith et al. 1998). A bright and prolonged outburst from this source lasted ~ 250 days, until 1999 May. During this time RXTE performed a series of pointed observations on a nearly daily basis. Extensive spectral and timing studies of this source have been performed using these data. The source has been observed in the “very high”, “intermediate”, and “high/soft” spectral states of black hole X-ray novae (Sobczak et al. 1999; Wijnands et al. 1999; Sobczak et al. 2000b; Homan et al. 2001). The X-ray spectrum usually displays two components that can be well modeled as thermal emission from an accretion disk ($kT \sim 1$ keV) and a power-law component that extends to at least 150 keV (Sobczak et al. 2000b). A summary of the observations, the values of the spectral parameters, and the integrated measures of the disk flux and the power-law flux are tabulated for all 209 observations during the 1998-1999 outburst in Sobczak et al. (2000b). Additional X-ray outbursts with significantly weaker maxima and shorter duration were observed with the ASM in 2000 April - June (Smith et al. 2000) and again in 2001 February - March (Tomsick et al. 2001).

Optical observations of XTE J1550–564 have revealed the binary period of 1.54 days (Jain et al. 2001). However, the optical mass function is not yet measured, and the source remains a black hole candidate on the basis of its X-ray timing and spectral characteristics. Radio observations have revealed evidence for a relativistic jet associated with the large X-ray flare of 1998 September 19 (Hannikainen et al. 2001). The radio flux subsequently decayed away while the X-ray source remained in the “very high” state. Weaker radio flux with an inverted spectrum was seen while the source was in the X-ray “low-hard” state during the outburst of 2000 (Corbel et al. 2001), and this has been interpreted to indicate the presence of a steady, compact jet at that time.

In some observations during the 1998-1999 outburst, the X-ray power spectra of XTE J1550–564 exhibit quasi-periodic oscillations (QPOs) at both high frequencies (HFQPOs; ~ 100 –285 Hz; Remillard et al. 1999; Homan et al. 2001) and low frequencies (LFQPOs; 0.08–18 Hz; Cui et al. 1999; Sobczak et al. 2000a). The LFQPOs are sometimes particularly strong, with peak to trough ratios as high as 1.5. (see Fig. 1 of Sobczak et al. 2000b). The latter study shows that the frequency and amplitude of QPOs below 20 Hz are correlated with both the power-law and the disk components in the X-ray spectrum. These QPOs are observed only when the power-law component contributes more than 20% of the 2–20 keV flux; at the same time, the QPO frequency is directly correlated with the amount of disk flux (unabsorbed) seen in the 2–20 keV band (Sobczak et al. 2000a).

Recent efforts to understand LFQPOs have turned attention to the phase lags associated with these oscillations and their harmonics. The analysis technique uses Fourier cross spectra to measure both the phase lags and the coherence parameter (versus frequency) between selected “soft” and “hard” X-ray energy bands. The results obtained for the first 13 RXTE observations of XTE J1550–564 showed unexpected phase lags in which the variations in hard X-ray preceded those in soft X-rays (Cui et al. 2000). Wijnands, Homan, & van der Klis (1999) used 14 observations of XTE J1550–564 near the end of the 1998-1999 outburst to begin organizing LFQPO properties in terms of two different QPO types. Their first type (“A”) is broad and exhibits a phase lag in soft X-rays; their second type (“B”) is narrower and exhibits hard lags in the strongest feature but soft lags in the harmonics.

In the present paper, we begin with an investigation of the phase lags associated with LFQPOs for all 209 RXTE observations of XTE J1550–564 that cover the 250 day outburst of the source during 1998-1999. We find three QPO types, one in addition to those reported by Wijnands et al. (1999). We then assess the correlations between the phase lags, other properties of LFQPOs, the X-ray spectral parameters, and also the properties of HFQPOs.

2. Observations and Data Analysis

Most of the PCA data were accumulated with $125\mu\text{s}$ resolution in “single bit” mode, providing two energy channels corresponding roughly to 2–6 and 6–13 keV, respectively (modes SB_125us_0_17_1s & SB_125us_18_35_1s). Above 13 keV, “event mode” was used with 16 energy channels and $16\mu\text{s}$ time resolution (mode E_16us_16B_36_1s). In this investigation the single-bit data and the event-mode data were each combined into a single channel, resulting in two energy bands covering 2–13 keV and 13–30 keV, respectively. We chose 13-30 keV for the “hard” band in order to isolate the power-law component and to select the channel (among the 3 choices) where the QPOs are often the strongest, in terms of percent amplitude. Different data modes forced us to use alternative channel boundaries for five of the observations, and the details are given in the footnotes to Table 1.

The power density spectra (PDS) were computed for XTE J1550–564 in the sum energy band (i.e. 2–30 keV), as described in Sobczak et al. (2000a). The power spectra and cross spectra, described below, were computed for every 256 s data segment. Then, for each observation we averaged together the results from the individual segments. Finally, the PDS for each observation are averaged in logarithmically increasing intervals of frequency (ν) prior to their display in units of log power density versus $\log \nu$.

We compute the phase lag and coherence function between the 2–13 keV and 13–30 keV energy bands as described in Bendat & Piersol (1986) and Vaughan & Nowak (1997). The coherence functions reported here include a correction for the effects of Poisson noise. When the coherence value is very low, then the measured phase lag cannot be trusted (see Nowak et al. 1999). To avoid showing meaningless results in Figs. 1–3, we refrain from plotting the phase lags and coherence at high frequency when the statistical uncertainty in the coherence function is near unity.

We detected LFQPOs (i.e. below 20 Hz) in 72 of the 209 PCA observations during 1998-1999; the results of our analysis of these QPOs are given in Table 1. For a majority of LFQPOs, the profiles show three peaks with frequencies in the ratio 1:2:4. In the final analysis we fit for the amplitude and FWHM of each peak individually, using Lorentzian functions. However, we used only one free parameter for the QPO frequency, which forced the central frequencies of the three peaks to be harmonically related, as indicated above. There were only 4 cases where the fit residuals indicated a slight yet significant departure from this harmonic relation (Obs. # 31, 43, 156, & 162; see Table 1). These results confirm that the peaks are harmonically related, and we suggest that the four exceptions are likely caused by the evolution of the QPO waveform during the observation in question.

2.1. The “Fundamental” QPO Feature

The top panels of Figures 1–3 show some representative power density spectra. Here we focus on the triple-peaked QPO profiles, which occur for most of the 72 cases reported in Table 1. The central peak with frequency ν_o strongly dominates over the satellite features, which occur at $0.5\nu_o$ and $2\nu_o$. If the lowest frequency, $0.5\nu_o$, is the fundamental frequency of the system, then the other two peaks correspond to the first and third harmonics, while there is no apparent feature at the second harmonic ($1.5\nu_o$). We derived upper limits for a peak at the second harmonic for five power spectra that have pronounced triple-peaked QPOs (Obs. # 52, 53, 54, 159, & 163; see Table 1) by adding another Lorentzian peak at $1.5\nu_o$ to the fitting model. No significant new detections were obtained. The statistical fluctuations produced candidate features with amplitudes (i.e. integrated rms power normalized to the mean count rate) that ranged from $< 0.1\%$ to $< 0.7\%$. The average of the five amplitudes, 0.4% , is very small compared to the corresponding amplitudes of the observed peaks at $0.5\nu_o$ and ν_o , which are greater by a factor of 5 and 10, respectively. Our failure to detect a second harmonic component suggests that $0.5\nu_o$ may not be the fundamental frequency of the system.

A second and perhaps more compelling reason to focus attention on the strongest QPO

feature is that there are time intervals in which the feature at $0.5 \nu_o$ gradually fades below the detection threshold, while the relative strength of the other peaks appears to remain constant. For example, consider observations # 3–14 in Table 1. The feature at $0.5 \nu_o$ falls in and out of detectability while the features at ν_o and $2\nu_o$ are continuously detected. This provides motivation to focus attention on the strongest QPO feature. On the other hand, if we were to redefine the fundamental QPO as the one detected with the lowest frequency, then we would find large variations in the relative amplitudes of the harmonics, and frequency discontinuities would appear in the correlation plots given below.

We therefore adopt an observational strategy and *presume* that the strongest QPO feature in XTE J1550–564 is the “fundamental”. From that perspective, the first harmonic is almost always present with a strength (relative to the fundamental) of roughly 0.1 to 0.5, similar to that of GRS1915+105 (see Munro, Morgan, & Remillard 1999). In 17% of the observations we fail to detect a peak at $0.5\nu_o$; however, its amplitude rises to 60% relative to the QPO at ν_o on some occasions (e.g. 1998 October 15). When we do detect the subharmonic, its Q value ($Q = \nu/FWHM$) is almost always less than the Q of the fundamental. Our identification of the dominant QPO peak with the fundamental frequency imposes a serious challenge to identify a physical mechanism that can generate X-ray power at $0.5\nu_o$; however, we regard this consequence as less of a problem than the alternative course. In the format for Table 1, we first list the LFQPO fundamental, and the frequency of any HFQPO is given in the last column on that line. The subsequent two lines report the properties of the first harmonic and then the subharmonic, if the detections are above 3σ .

2.2. Broadband Features in the Power Continuum

The relationship between QPO frequencies and the frequencies of other broad features or spectral breaks in the power continuum have been investigated by Wijnands & van der Klis (1999) and Psaltis, Belloni & van der Klis (1999). They report frequency correlations and argue that the accreting black holes and neutron stars exhibit essentially similar patterns of PDS variability. The results were interpreted in terms of a relativistic precession model that applies to compact objects of both types (Stella, Vietri, & Morsink 1999).

We have investigated this topic for the case of XTE J1550–564, using all of the observations during the 1998–1999 outburst. There are broad features in the power continuum, with $Q < 1$, and we have attempted to measure these by identifying either the breaks in the PDS (assuming power law functions for the frequency intervals between the breaks), or by fitting for peaks in the $(\nu \times PDS_\nu)$ vs. ν plane. In both cases, we find systematic problems that prevent us from drawing any firm conclusions. We have

also investigated the relationship between LFQPOs and HFQPOs, both of which generally pertain to PDS features with $Q > 2$, and we report those results in Section 3.2 below.

In our attempts to define breaks in the power continuum, we find that we cannot obtain a satisfactory fit for all of the power spectra using one mathematical model. Many of the power spectra during the early phase of the outburst (see Fig. 2 in Cui et al. 1999) are well fit above 0.1 Hz by a model consisting of two continuum breaks and a QPO with one harmonic. However, in other observations, e.g during 1998 September 15-22 (see Fig. 1 in Remillard et al. 1999), three to five continuum breaks are required.

The broad features in the power continuum of XTE J1550–564 are most apparent as peaks in the $(\nu \times PDS_\nu)$ vs. ν plane (Psaltis, Belloni & van der Klis 1999). We find that there are generally one to three broad peaks per observation, and the profiles of these peaks often deviate from simple mathematical models. The LFQPOs may or may not lie near the center of one peak. Further progress on this analysis topic requires additional efforts to solve the modeling problems and to devise selection criteria to guide the comparison of broad features and QPO detections. Such tasks are beyond the scope of this paper, and we are presently unable to derive useful conclusions regarding the relationship between the QPO frequencies and the broadband peaks and breaks in the power continuum for XTE J1550–564.

3. Results

3.1. QPO Types

We find three fundamental types of phase lag behavior for XTE J1550–564. Figures 1 and 2 show representative power density spectra, phase lags, and coherence functions for the three types of QPOs. Types A and B correspond to those identified previously by Wijnands et al. (1999), while type C QPOs (narrow, with soft phase lags) appear during the first half of the outburst in observations that they did not analyze. In addition to types A, B and C, anomalous QPOs were observed on two occasions, and their power spectra are shown in Fig. 3.

Type A timing behavior is characterized by a broad QPO ($Q \sim 2-3$) near 6 Hz that appears to be a superposition of the fundamental and the first harmonic (Fig. 1). The integrated rms amplitude of the QPO features is a few percent. The phase lags for type A behavior are generally featureless except for a broad soft lag centered near the QPO feature with $|\Delta\phi| \sim 1$ rad and poor coherence ($< 50\%$). We identify four observations with type A QPO behavior, all of which display HFQPOs in the range 270-284 Hz (see Table 1). There

are six additional observations in which the QPO is broad but the statistics are inadequate to establish a soft phase lag. These are labeled “A?”, and they include the last three QPO detections (Table 1) in which the QPO is only evident above 6 keV. Of the six “A?” cases, an additional four have HFQPOs in the range 214–284 Hz. Typically, the HFQPOs have $Q \sim 10$, and they are maximally detected by ignoring the PCA counts below 6 keV.

Type B QPO behavior is characterized in the 1998 October 20 observation (Fig. 1) by a narrow fundamental QPO feature ($Q \sim 10$) at 5.5 Hz (see Fig. 1) with rms amplitude of 3.5%. Type B observations display a hard lag ($\Delta\phi \sim 0.0$ – 0.4 rad) that is slightly shifted from the fundamental feature, while there are soft lags associated with the first and subharmonics. The coherence of the type B QPO is typically within 10% of unity. Type B QPOs also have strong subharmonics that are typically 30–60% of the amplitude of the fundamental. We identify 9 observations with type B QPO behavior. Six of these additionally display HFQPOs in the range 182–209 Hz. These HFQPOs are systematically lower in frequency compared to the type A group, they are broader in width ($Q \sim 5$), and their amplitude is more broadly distributed with X-ray photon energy.

We introduce type C timing behavior in Fig. 2. The 1998 October 10 observation (Obs. #43) also happens to be one of the four previously noted cases in which the harmonics are slightly shifted from the expected positions, shown with dashed lines in the left panel of Fig. 2. The slight frequency offsets are barely discernible in logarithmic units. Type C QPOs occur primarily during the first half of the outburst, when the source is in the very high state and the power-law component contributes $\gtrsim 75\%$ of the 2–20 keV flux (Sobczak et al. 2000b). Type C timing behavior is characterized by sharp ($Q \gtrsim 10$) fundamental QPO features with a range of rms amplitudes from 3–16%. The first harmonic is present, and the first subharmonic is usually observed as well. The phase lags for type C behavior are typically modest, with the fundamental exhibiting soft lags $|\Delta\phi| \lesssim 0.4$ rad. The subharmonic usually has a small soft phase lag of the same magnitude as the fundamental, whereas, the first harmonic has a hard lag, which can be several times larger than the soft lag displayed by the fundamental. The coherence of the fundamental is high ~ 85 – 95% , while the coherence of the first and subharmonic is typically closer to 75–80%. We identify 51 observations with type C QPO behavior. Only five of these display HFQPOs, and their frequencies are all below 170 Hz.

Among the 51 observations of type C QPOs, there are 5 cases that are distinguished by weak harmonics and a double-peak structure within the profile of the fundamental. An example is shown in Fig. 2. These five cases are labeled “C’” in Table 1; they all occur during the two days (1998 September 20–21) immediately following the 6.8 Crab flare in the XTE J1550–564 light curve. If we divide any of these observations into smaller time

intervals, we find a single narrower QPO, suggesting that the QPO shifts in frequency during the observation. The harmonics are difficult to discern for type C' QPOs; nevertheless, there is significant structure in the phase lag near the harmonic frequencies (see the dotted vertical lines in Fig. 2). Apart from their PDS profiles, the C' QPOs exhibit properties that overlap with the other type C cases: frequencies from 6–10 Hz, rms amplitudes of 3–7%, and phase lags ~ -0.2 rad. Therefore, in our judgment, the C' QPOs are best described as type C QPOs with frequency shifts that are probably related to the system's recovery from the huge X-ray flare that preceded those observations.

The properties of the three fundamental types of LFQPOs in XTE J1550–564 are summarized in Table 2. There are two observations that do not conform to these QPO categories, and they are shown in Fig. 3. The first anomalous QPO occurred during the 6.8 Crab flare on 1998 September 19 (Sobczak et al. 1999). This observation produced a 13 Hz QPO with an integrated rms amplitude of 1%, a large soft lag of -0.9 ± 0.2 rad, and a coherence of $80 \pm 20\%$. The power-law dominates the spectrum during this flare, with the disk contributing only $\sim 3\%$ of the 2–20 keV flux. The magnitude of the soft phase lag is consistent with type A behavior; however, the presence of a QPO at 183 Hz resembles type B cases, but the LFQPO frequency and the low fractional contribution of the disk flux is similar to type C behavior. The second anomalous QPO occurred on 1999 March 2. This LFQPO (18 Hz) is observed at a much higher frequency than the others, while the coherence at all frequencies is very low. It is significantly sharper than the other LFQPOs ($Q \sim 19$) and has a very small rms amplitude (0.5%) with no harmonics.

3.2. Correlations with the Accretion Disk and High-Frequency QPOs

We use the measured QPO properties (Table 1) to investigate the relationship between the phase lag and the frequency and amplitude of the fundamental feature. The results are shown in Fig. 4, where we use different plotting symbols to identify the QPO type. The relationships clearly appear more organized when the QPO type is distinguished. For type C QPOs, as the phase lag decreases below zero (i.e. increasing soft lag), the QPO frequency increases and the amplitude decreases.

In Fig. 5, we examine how the QPO parameters vary in response to the observed spectral changes in the X-ray component attributed to the accretion disk. In the left panels of Fig. 5, we plot the LFQPO parameters versus the disk color temperature, using the spectral parameters given in Table 2 of Sobczak et al. (2000b). Again, the results appear more organized when the QPO type is distinguished. In the central panels in Fig. 5 we plot the QPO parameters versus the unabsorbed disk flux, here restricting the integration

over photon energy to the range 2-20 keV, as given in Table 3 of Sobczak et al. (2000b) . There is a very striking linear correlation between the QPO frequency and the amount of disk flux that falls within the bandwidth of the PCA instrument. In the right panels, the QPO parameters are plotted versus the bolometric disk flux: $f_{abb} = 2.16 \times 10^{-11} NT^4$ erg cm⁻² s⁻¹, where N and T are the normalization and color temperature, respectively, for the accretion disk, as derived from the X-ray spectral analyses. Compared to the central panels in Fig. 5, the increased scatter in the right panels is probably a consequence of the fact that most of the disk flux is below 2 keV. Thus the calculation of the total disk flux requires extrapolation of the spectrum well below the threshold of the PCA instrument, and even small statistical or systematic errors in the temperature measurement may cause significant errors in the calculation of the bolometric disk flux. Alternatively, we cannot exclude the possibility that the thermal X-ray component actually diverges from the simple disk blackbody model at low photon energies.

Overall, the frequency of type C QPOs is most correlated with the disk flux, while the QPO amplitude and phase lags show slightly greater correlation with the disk temperature (see Fig. 5). We further note that while the sequence of QPO types C \rightarrow B \rightarrow A is associated with increased total disk luminosity, the disk’s contribution to the total flux decreases along this sequence, and the total luminosity is greatest when we observe the huge flare of 1998 September 19 (with an anomalous QPO) and the subsequent decay with type C’ QPOs. We have plotted the QPO parameters versus the spectral properties of the power-law component (not shown), and the results produce only rough correlations, with increased scatter compared to the left and right panels of Fig. 5.

In Fig. 6, we examine the phase lag of LFQPOs versus the fraction of the unabsorbed flux contributed by the accretion disk. The disk fraction is calculated in two ways, analogous to the central and right panels of Fig. 5. In the left panel of Fig. 6, the flux for both spectral components is integrated over the range 2–20 keV. In the right panel we consider the entire disk-blackbody spectrum, and we integrate the power-law component over the range 1–30 keV. The intent of the latter method is to track the bolometric flux from each spectral component, but the calculations are subject to increased systematic uncertainty, as noted with respect to Fig. 5. The results show that each types of QPO occupies a distinct region in Fig. 6. The situation is clearest in the left panel where the three types of QPOs segregate into distinct regions: the C type QPOs occur when the fraction $\lesssim 0.26$, type A QPOs occur when the disk fraction $\gtrsim 0.37$, and type B QPOs occur when the disk fraction lies between these values. We further note that QPOs are not detected for the majority of observations in which the disk fraction exceeds 0.4 (or 0.5 for bolometric fraction), and there is only a one (peculiar) QPO detection when the disk fraction exceeds 0.8.

Finally, for the 20 observations with HFQPOs listed in Table 1, we plot the frequencies of HFQPOs versus the LFQPO fundamental in the top panel of Fig. 7; the frequencies appear to be uncorrelated. A weak correlation would be produced if we plot the LFQPO frequencies at $0.5\nu_0$ for types B and C only, but our reasons for not doing so are given in Section 2.1. However, in the same plot we do see a clear relation between LFQPOs and HFQPOs in that the symbol type changes progressively with the frequency of the HFQPO. All of the high- Q detections near 283 Hz are associated with broad, type A QPOs at 5-10 Hz, while the cluster of broader QPOs near 183 Hz mostly occur with more narrow, type B QPOs at 5-7 Hz. The trend toward an anti-correlation in the Q values ($\nu/FWHM$) of HFQPOs and LFQPOs is shown in the bottom plot of Fig. 7. We further note that the amplitude of the fundamental feature decreases with types A and B (see Fig. 5), when HFQPOs are frequently detected. Using the results given in Table 1, it can be seen that the LFQPO amplitudes are generally (19 of 20 cases) in the range 1–8% when HFQPOs are detected, but when HFQPOs are not detected the LFQPO amplitude is generally (43 of 52 cases) in the range of 8–16%. We conclude that the amplitudes of LFQPOs and HFQPOs also appear to be anti-correlated in XTE J1550–564.

4. Discussion

We have shown that the effort to distinguish QPO types by their measured phase lag and coherence is useful in sorting out the properties of LFQPOs; furthermore, it provides insight into the relationship between LFQPOs and HFQPOs in XTE J1550-564. The QPO types also help to establish certain strong correlations between the properties of the type C oscillations and the spectral properties of the accretion disk. These correlations, particularly the one in the top-central panel of Fig. 5, also provide assurance that the spectral deconvolution of the two spectral components (i.e. thermal and power law) using the RXTE PCA instrument is physically meaningful, and this should encourage more sophisticated disk models that may allow us to interpret the physical conditions in the inner disk without the uncertainties inherent in the simple multi-temperature disk model.

Coherence functions and phase lags are expected to provide powerful constraints on the X-ray power-law component of accreting black holes when interpreted with a physical model for Comptonization. In the extended corona model (e.g. Miyamoto et al. 1988; Hua & Titarchuk 1996; Kazanas, Hua & Titarchuk 1997; Nowak et al. 1999), the hard photons undergo more scatterings in order to reach higher energies and therefore lag behind the soft photons in the response to flares from the inner accretion disk. The hard lag is directly related to the photon diffusion time scale through the corona, which scales logarithmically

with photon energy (Hua & Titarchuk 1996), in agreement with some observations (Cui et al. 1997; Nowak et al. 1999). This scenario has been invoked to constrain the structure of an extended but inhomogeneous Compton corona (Kazanas & Hua 1999). However, problems accommodating large observed phase lags have prompted alternative models in which the lags signify the spectral and temporal evolution of the parent mechanism of Comptonization. This may occur, e.g., with magnetic loop structures in the disk (Poutanen & Fabian 1999), where the hot plasma associated with magnetic instabilities may produce secondary effects such as disk heating and Comptonization.

The topic of QPO phase lags and coherence measures is especially difficult because one must deal with an unknown oscillation mechanism. When LFQPOs are detected there is always a substantial X-ray power law, but the relationship between the QPOs and the X-ray spectral components is very complicated, as shown herein and elsewhere (e.g. Markwardt, Swank, & Taam 1999; Munro, Morgan, & Remillard 1999; Sobczak et al. 2000a). The model for Comptonization via bulk motion flow does predict a correlation between disk flux and QPO frequency (Titarchuk, Lapidus, & Muslimov 1998); however, the applicability of this model to LFQPO below 20 Hz is questionable, and the measured soft lags appear to be problematic. A proposal to explain QPO phase lags in GRS 1915+105 has been offered by Nobili et al. (2000), who invoke radial oscillations in a transition boundary between the disk and an inner Comptonizing region. However, their model does not accommodate the wealth of observational evidence presented herein and in similar RXTE studies.

It is clear, e.g. in Figs. 1-3, that the plots of phase lags and coherence functions show features that coincide with the profiles of the QPOs and harmonics. The contrast between the QPOs and the broadband power continuum, along with the sign reversals in the QPO phase lags, might signify less about Comptonization and more about the details of the QPO waveform. Similar sign reversals in phase lags were also reported for LFQPOs in the microquasar and black hole candidate GRS 1915+105 (Cui 1999; Reig et al. 2000; Munro et al. 2001). Further insights regarding the QPO waveforms and their physical origin might come from "QPO-folding" analyses such as those undertaken by Morgan, Remillard, & Greiner (1997).

HFQPOs are coincident with almost all type A and B LFQPOs and rarely with QPOs of type C. The frequencies of the fast and slow QPOs in XTE J1550-564 do not appear to be correlated, casting some doubt on the relationship proposed to unite the QPOs in both neutron-star and black-hole systems (Psaltis, Belloni & van der Klis 1999). On the other hand there does appear to be evidence of a connection between LFQPOs and HFQPOs in the sense of an anti-correlation between their amplitudes and Q values. These comparisons are bounded by the disappearance of all QPOs when the disk contributes more than $\sim 80\%$

of the flux. On the other hand there is a low probability of detecting HFQPOs when the disk contributes less than $\sim 30\%$ of the total flux *and* the LFQPO amplitude is above 8%. Taken as a whole, our results suggest that both LFQPOs and HFQPOs arise in the inner accretion disk, that the power-law component is associated with the excitation of these oscillations, and that there is some mutual antagonism in the structures that are responsible for HFQPOs and LFQPOs, respectively. The accretion-ejection instability in magnetized disks (Tagger & Pellat 1999) is one example of a mechanism that could cause such an effect. It is proposed that LFQPOs occur when the instability forms a standing spiral wave that transfers energy from the inner disk to larger radii. As the amplitude of the wave increases, it is conceivable that the LFQPO amplitude would increase while energy depletion in the inner disk might weaken the HFQPO.

We thank E. Morgan, J. Homan, and R. Wijnands for helpful discussions. Partial support for R.R. and M.M. was provided by the NASA contract to M.I.T. for RXTE instruments, and for J.M. and G.S. by NASA Grant NAG5-10813.

REFERENCES

- Bendat, J. & Piersol, A. 1986, *Random Data: Analysis and Measurement Procedures* (New York: Wiley)
- Corbel, S. et al. 2001, *ApJ*, in press; astro-ph/0102114
- Cui, W. 1999, *ApJ*, 524, L59
- Cui, W., Zhang, S. N. & Chen, W. 2000, *ApJ*, 531, L45
- Cui, W., Zhang, S. N., Chen, W., & Morgan, E. H. 1999, *ApJ*, 512, L43
- Cui, W., Zhang, S. N., Focke, W., & Swank, J. H. 1997, *ApJ*, 484, 383
- Hannikainen, D., Wu, K., Campbell-Wilson, D., Hunstead, R., Lovell, J., McIntyre, V., Reynolds, J., Soria, T., & Tzioumis, T. 2001, *Procs. 4th INTEGRAL Workshop*, in press; astro-ph/0102070
- Homan, J., Wijnands, R., van der Klis, M., Belloni, T., van Paradijs, J., Klein-Wolt, M., Fender, R., & Méndez, M. 2001, *ApJS*, 132, 377
- Hua, X.-M. & Titarchuk, L. 1996, *ApJ*, 496, 280

- Jain, R., Bailyn, C. D., Orosz, J. A., McClintock, J. E., Sobczak, G. J., & Remillard, R. A. 2001, *ApJ*, 546, 1086
- Kazanas, D. & Hua, X.-M. 1999, *ApJ*, 519, 750
- Kazanas, D., Hua, X.-M., & Titarchuk, L. 1997, *ApJ*, 480, 735
- Levine, A. M., Bradt, H., Cui, W., Jernigan, J. G., Morgan, E. H., Remillard, R., Shirey, R. E., & Smith, D. A. 1996, *ApJ*, 469, 33
- Markwardt, C. B., Swank, J. H., & Taam, R. E. 1999, *ApJ*, 513, L37
- Miyamoto, S., Kitamoto, S., Mitsuda, K., & Dotani, T. 1988 *Nature*, 336, 450
- Morgan, E. H., Remillard, R. A., & Greiner, J. 1997, *ApJ*, 482, 993
- Muno, M. P., Morgan, E. H., & Remillard, R. A. 1999
- Muno, M. P., Remillard, R. A., Morgan, E. H., Waltman, E. B., Dhawan, V., Hjellming, R. M., & Pooley, G. 2001, *ApJ*, in press; astro-ph/0104067
- Nobili, L., Turolla, R., Zampieri, L., & Belloni, T. 2000, *ApJ*, 538, L137
- Nowak, M. A., Vaughan, B. A., Wilms, J., Dove, J. B., & Begelman, M. C. 1999, *ApJ*, 510, 874
- Psaltis, D., Belloni, T., & van der Klis, M. 1999, *ApJ*, 520, 262
- Poutanen, J. & Fabian, A. C. 1999, *MNRAS*, 306, L31
- Reig, P., Belloni, T., van der Klis, M., Mendez, M., Kylafis, N. D., & Ford, E. C. 2000, *ApJ*, 541, 883
- Remillard, R. A., McClintock, J. E., Sobczak, G. J., Bailyn, C. D., Orosz, J. A., Morgan, E. H., & Levine, A. M. 1999, *ApJ*, 517, L127
- Smith, D. A. & RXTE/ASM teams 1998, *IAU Circ.*7008
- Smith, D. A., Levine, A. M., Remillard, R. A., Fox, D., & Shaefer, R. 2000, *IAU Circ.*7399
- Sobczak, G. J., McClintock, J. E., Remillard, R. A., Levine, A. M., Morgan, E. H., Bailyn, C. D., & Orosz, J. A. 1999, *ApJ*, 517, L121
- Sobczak, G. J., McClintock, J. E., Remillard, R. A., Cui, W., Levine, A. M., Morgan, E. H., Orosz, J. A., & Bailyn, C. D. 2000a, *ApJ*, 531, 537

- Sobczak, G. J., McClintock, J. E., Remillard, R. A., Cui, W., Levine, A. M., Morgan, E. H., Orosz, J. A., & Bailyn, C. D. 2000b, *ApJ*, 544, 993
- Stella, L., Vietri, M., & Morsink, S. M. 1999, *ApJ*, 524, L63
- Tagger, M. & Pellat, R. 1999, *â*, 349, 1003
- Titarchuk, L., Lapidus, I., & Muslimov, A. 1998, *ApJ*, 499, 315
- Tomsick, J. A., Smith, D. A., Swank, J. H., Wijnands, R., & Homan, J. 2001, *IAU Circ.*7575
- Vaughan, B. A. & Nowak, M. A. 1997, *ApJ*, 474, L43
- Wijnands, R., Homan, J., & van der Klis, M. 1999, *ApJ*, 526, 33
- Wijnands, R. & van der Klis, M. 1999, *ApJ*, 514, 939

Table 1. Low-Frequency QPO Parameters for XTE J1550–564: Fundamental and Harmonic Frequencies

Obs #	Date (yyymmdd)	MJD ^a	Type	QPO ν^b (Hz)	Amplitude ^c (% rms)	Q ^d	Phase Lag ^e (radians)	Coherence ^f	HFQPO ^g (Hz)
1	980907	51063.72	C	0.081	13.1 ± 1.4	16.2	0.10 ± 0.22	0.95 ± 0.04	...
...	0.16	11.5 ± 0.9	7.9	0.11 ± 0.20	0.99 ± 0.03	...
2	980908	51064.01	C	0.122	12.3 ± 0.7	8.7	−0.03 ± 0.01	0.997 ± 0.002	...
...	0.24	8.0 ± 0.6	5.2	0.08 ± 0.02	0.995 ± 0.003	...
3	980909	51065.07	C	0.288	14.6 ± 0.9	16.9	−0.01 ± 0.01	0.994 ± 0.003	...
...	0.58	5.1 ± 0.4	12.5	0.10 ± 0.03	0.965 ± 0.008	...
...	0.14	3.8 ± 0.5	6.8	−0.04 ± 0.03	0.965 ± 0.010	...
4	980909	51065.34	C	0.395	13.5 ± 0.8	13.6	−0.02 ± 0.02	0.985 ± 0.004	...
...	0.79	6.1 ± 0.6	9.1	0.09 ± 0.05	0.948 ± 0.015	...
5	980910	51066.07	C	0.81	14.3 ± 0.5	13.1	0.05 ± 0.02	0.971 ± 0.005	...
...	1.6	5.9 ± 0.4	8.4	0.16 ± 0.04	0.888 ± 0.017	...
6	980910	51066.34	C	1.03	15.0 ± 0.4	12.5	0.02 ± 0.02	0.962 ± 0.007	...
...	2.1	6.5 ± 0.3	7.5	0.11 ± 0.04	0.884 ± 0.018	...
7	980911	51067.27	C	1.54	15.1 ± 0.4	11.2	0.04 ± 0.01	0.971 ± 0.004	...
...	3.1	5.0 ± 0.2	10.5	0.23 ± 0.04	0.801 ± 0.021	...
8	980912	51068.35	C	2.38	13.7 ± 0.4	12.6	0.01 ± 0.01	0.963 ± 0.004	...
...	4.8	5.3 ± 0.2	9.6	0.24 ± 0.05	0.765 ± 0.026	...
...	1.2	2.7 ± 0.3	4.8	0.02 ± 0.06	0.777 ± 0.033	...
9	980913	51069.27	C	3.33	12.8 ± 0.3	15.1	−0.04 ± 0.01	0.974 ± 0.003	...
...	6.7	4.0 ± 0.2	14.5	0.31 ± 0.05	0.759 ± 0.030	...
...	1.7	2.2 ± 0.3	7.2	−0.06 ± 0.05	0.770 ± 0.028	...
10	980914	51070.13	C	3.20	13.1 ± 0.3	16.0	−0.03 ± 0.01	0.969 ± 0.003	...
...	6.4	4.2 ± 0.2	13.9	0.30 ± 0.04	0.655 ± 0.026	...
11	980914	51070.27	C	3.17	13.0 ± 0.3 ^j	21.1	−0.03 ± 0.02	0.959 ± 0.004	...
...	6.3	4.0 ± 0.2	11.5	0.38 ± 0.05	0.652 ± 0.027	...
12	980915	51071.20	C	3.69	12.2 ± 0.2 ^j	14.8	0.00 ± 0.01	0.971 ± 0.003	...
...	7.4	3.8 ± 0.2	12.9	0.34 ± 0.05	0.710 ± 0.035	...
13	980915	51072.00	C	2.58	14.7 ± 0.7	23.5	0.08 ± 0.04	0.976 ± 0.040	...
...	5.1	5.2 ± 0.3	17.2	0.35 ± 0.06	0.794 ± 0.033	...
...	1.3	2.8 ± 0.3	7.9	0.22 ± 0.09	0.682 ± 0.058	...

Table 1—Continued

Obs #	Date (yymmdd)	MJD ^a	Type	QPO ν^b (Hz)	Amplitude ^c (% rms)	Q ^d	Phase Lag ^e (radians)	Coherence ^f	HFQPO ^g (Hz)
14	980916	51072.34	C	4.02	11.9 ± 0.2	15.5	−0.07 ± 0.02	0.965 ± 0.004	...
...	8.0	3.3 ± 0.2	14.6	0.29 ± 0.05	0.687 ± 0.03	...
...	2.0	2.6 ± 0.3	11.1	−0.08 ± 0.05	0.763 ± 0.031	...
15	980918	51074.14	C	5.75	8.8 ± 0.2	9.6	−0.163 ± 0.02	0.927 ± 0.007	...
...	11.5	1.3 ± 0.1	12.4	0.02 ± 0.07	0.638 ± 0.055	...
...	2.9	1.8 ± 0.2	7.4	−0.14 ± 0.05	0.860 ± 0.024	...
16*	980919	51075.99	?	13.2	0.8 ± 0.1	5.0	−1.02 ± 0.12	0.82 ± 0.15	183 ± 4
...	4.9	0.26 ± 0.03	14.6	−0.40 ± 0.13	0.97 ± 0.21	...
17	980920	51076.80	C ^j	7.2	6.6 ± 0.1 ^j	5.0	−0.22 ± 0.02	0.859 ± 0.009	...
18 ^h	980920	51076.95	C ^j	8.5	4.8 ± 0.1 ^j	4.3	−0.23 ± 0.02	0.883 ± 0.009	...
19 ^h	980921	51077.14	C ^j	9.8	3.2 ± 0.1	9.2	−0.17 ± 0.02	0.883 ± 0.014	169 ± 5
...	19.6	1.2 ± 0.1	5.0	0.07 ± 0.16	0.71 ± 0.18	...
20 ^h	980921	51077.21	C ^j	7.1	4.0 ± 0.1 ^k	5.4	−0.19 ± 0.02	0.875 ± 0.009	159 ± 4
21	980921	51077.87	C ^j	6.3	10.2 ± 0.4 ^k	5.8	−0.15 ± 0.02	0.901 ± 0.005	...
22	980922	51078.13	C	5.41	9.7 ± 0.1 ^j	11.3	−0.15 ± 0.02	0.927 ± 0.005	...
...	10.8	2.1 ± 0.2	13.0	0.25 ± 0.04	0.692 ± 0.037	...
...	2.7	1.6 ± 0.2	5.0	−0.13 ± 0.03	0.870 ± 0.015	...
23 ⁱ	980923	51079.79	C	3.90	12.1 ± 0.3	13.9	−0.04 ± 0.03	0.898 ± 0.012	...
...	7.8	3.3 ± 0.2	12.6	0.25 ± 0.10	0.521 ± 0.079	...
24 ⁱ	980924	51080.08	C	3.87	11.9 ± 0.2	14.3	−0.10 ± 0.02	0.931 ± 0.008	...
...	7.7	3.1 ± 0.2	13.3	0.42 ± 0.10	0.450 ± 0.070	...
...	1.9	2.1 ± 0.2	6.9	0.07 ± 0.06	0.740 ± 0.041	...
25	980925	51081.06	C	2.88	12.7 ± 0.2	10.7	−0.01 ± 0.01	0.978 ± 0.003	...
...	5.8	4.0 ± 0.2	10.3	0.25 ± 0.04	0.724 ± 0.020	...
...	1.4	2.3 ± 0.2	8.4	0.02 ± 0.04	0.784 ± 0.23	...
26	980926	51082.00	C	2.72	13.6 ± 0.2	10.9	−0.01 ± 0.01	0.973 ± 0.020	...
...	5.4	4.4 ± 0.2	12.1	0.23 ± 0.02	0.810 ± 0.015	...
...	1.4	2.0 ± 0.2	10.4	0.06 ± 0.03	0.769 ± 0.019	...
27	980927	51083.00	C	2.66	13.7 ± 0.2	9.8	−0.01 ± 0.01	0.966 ± 0.003	...
...	5.3	4.5 ± 0.2	10.8	0.22 ± 0.04	0.762 ± 0.021	...
...	1.3	1.8 ± 0.2	10.2	0.06 ± 0.04	0.816 ± 0.022	...
28	980928	51084.34	C	2.69	13.9 ± 0.2	11.2	−0.02 ± 0.01	0.970 ± 0.003	...
...	5.4	5.0 ± 0.2	8.1	0.22 ± 0.03	0.709 ± 0.020	...
...	1.3	2.6 ± 0.3	8.9	0.00 ± 0.05	0.741 ± 0.026	...
29	980929	51085.27	C	4.13	11.8 ± 0.2 ^j	12.9	−0.08 ± 0.01	0.962 ± 0.003	...
...	8.3	3.2 ± 0.1	10.0	0.26 ± 0.04	0.693 ± 0.025	...
...	2.1	1.8 ± 0.1	8.6	−0.10 ± 0.04	0.835 ± 0.017	...
30	980929	51085.92	C	2.89	14.0 ± 0.3	9.9	−0.04 ± 0.02	0.975 ± 0.004	...
...	5.8	3.9 ± 0.2	13.4	0.22 ± 0.05	0.796 ± 0.032	...
...	1.4	2.6 ± 0.3	6.5	0.03 ± 0.06	0.770 ± 0.038	...
31	980929	51085.99	C	3.09	13.3 ± 0.2 ^j	7.5	−0.04 ± 0.01	0.951 ± 0.004	...
...	6.1	4.1 ± 0.1 ^j	8.0	0.18 ± 0.03	0.730 ± 0.021	...
...	1.5	2.8 ± 0.2 ^j	6.2	0.02 ± 0.04	0.775 ± 0.023	...
32	980930	51086.89	C	3.51	12.5 ± 0.1 ^j	10.6	−0.06 ± 0.01	0.961 ± 0.002	...
...	7.0	3.7 ± 0.1	10.5	0.20 ± 0.02	0.727 ± 0.016	...
...	1.8	3.0 ± 0.1	6.3	0.02 ± 0.02	0.798 ± 0.014	...
33	981001	51087.72	C	3.44	12.9 ± 0.2 ^j	11.1	−0.05 ± 0.01	0.964 ± 0.002	...
...	6.9	3.8 ± 0.1	9.9	0.20 ± 0.02	0.765 ± 0.017	...
...	1.7	3.4 ± 0.2	6.8	0.02 ± 0.03	0.816 ± 0.015	...
34	981002	51088.01	C	3.21	13.3 ± 0.2	10.7	−0.06 ± 0.01	0.968 ± 0.003	...
...	6.4	4.0 ± 0.2	10.3	0.19 ± 0.03	0.775 ± 0.020	...
...	1.6	3.2 ± 0.2	6.4	0.01 ± 0.03	0.812 ± 0.017	...

Table 1—Continued

Obs #	Date (yyymmdd)	MJD ^a	Type	QPO ν^b (Hz)	Amplitude ^c (% rms)	Q ^d	Phase Lag ^e (radians)	Coherence ^f	HFQPO ^g (Hz)
35	981003	51089.01	C	3.04	14.1 ± 0.2	9.2	−0.06 ± 0.01	0.975 ± 0.003	...
...	6.1	3.3 ± 0.2	15.2	0.21 ± 0.04	0.784 ± 0.025	...
...	1.5	3.3 ± 0.3	6.9	0.05 ± 0.04	0.801 ± 0.026	...
36	981004	51090.14	C	3.93	12.4 ± 0.2	12.3	−0.08 ± 0.01	0.965 ± 0.003	...
...	7.9	3.5 ± 0.2	10.9	0.20 ± 0.05	0.784 ± 0.041	...
...	2.0	3.4 ± 0.2	5.8	−0.02 ± 0.03	0.849 ± 0.019	...
37	981004	51090.70	C	3.72	12.6 ± 0.2	11.6	−0.08 ± 0.01	0.963 ± 0.003	...
...	7.4	3.8 ± 0.1	9.8	0.19 ± 0.04	0.700 ± 0.028	...
...	1.9	3.6 ± 0.2	5.5	−0.11 ± 0.04	0.843 ± 0.020	...
38	981005	51091.74	C	5.60	10.3 ± 0.2	10.2	−0.15 ± 0.02	0.939 ± 0.006	...
...	11.2	2.2 ± 0.1	12.9	0.26 ± 0.07	0.605 ± 0.078	...
...	2.8	3.7 ± 0.2	3.8	−0.14 ± 0.05	0.881 ± 0.029	...
39	981007	51093.14	C	6.55	7.6 ± 0.1	10.6	−0.23 ± 0.02	0.896 ± 0.008	...
...	13.1	1.3 ± 0.2	11.5	0.29 ± 0.08	0.477 ± 0.050	...
...	3.3	2.4 ± 0.2	5.6	−0.23 ± 0.04	0.827 ± 0.021	...
40	981008	51094.14	C	4.32	12.0 ± 0.2	12.7	−0.10 ± 0.02	0.965 ± 0.004	...
...	8.6	3.4 ± 0.2	12.1	0.22 ± 0.05	0.780 ± 0.061	...
...	2.2	3.8 ± 0.2	5.1	−0.04 ± 0.05	0.848 ± 0.029	...
41	981008	51094.57	C	5.07	10.7 ± 0.2	12.7	−0.16 ± 0.02	0.950 ± 0.004	...
...	10.1	2.7 ± 0.2	12.1	0.23 ± 0.05	0.613 ± 0.038	...
...	2.5	3.7 ± 0.2	5.1	−0.05 ± 0.04	0.823 ± 0.031	...
42	981009	51095.61	C	4.49	11.9 ± 0.3	12.5	−0.13 ± 0.02	0.96 ± 0.01	...
...	8.9	4.1 ± 0.2	7.7	0.27 ± 0.07	0.73 ± 0.06	...
...	2.2	3.5 ± 0.2	7.5	0.00 ± 0.05	0.83 ± 0.03	...
43	981010	51096.57	C	5.40	11.7 ± 0.2 ^j	4.0	−0.12 ± 0.02	0.91 ± 0.01	...
...	10.2	4.9 ± 0.2 ^j	4.0	0.26 ± 0.05	0.60 ± 0.03	...
...	2.8	4.9 ± 0.2 ^j	4.0	−0.10 ± 0.03	0.84 ± 0.02	...
44	981011	51097.57	C	4.74	11.2 ± 0.3	11.6	−0.13 ± 0.02	0.95 ± 0.01	...
...	9.5	3.0 ± 0.2	11.0	0.39 ± 0.07	0.74 ± 0.06	...
...	2.4	4.1 ± 0.2	5.5	−0.04 ± 0.05	0.92 ± 0.02	...
45	981011	51097.81	C	4.20	12.7 ± 0.3	11.4	−0.14 ± 0.03	0.96 ± 0.01	...
...	8.4	3.8 ± 0.3	11.1	0.33 ± 0.08	0.82 ± 0.07	...
...	2.1	3.8 ± 0.3	7.0	0.05 ± 0.08	0.78 ± 0.04	...
46	981012	51098.28	C	5.00	12.0 ± 0.2	7.5	−0.17 ± 0.03	0.96 ± 0.01	...
...	10.0	4.6 ± 0.2	5.2	0.21 ± 0.06	0.77 ± 0.06	...
...	2.5	5.5 ± 0.2	4.4	−0.10 ± 0.06	0.85 ± 0.03	...
47	981013	51099.21	C	4.85	11.0 ± 0.2	11.8	−0.15 ± 0.02	0.95 ± 0.11	...
...	9.7	3.0 ± 0.2	11.5	0.52 ± 0.08	0.74 ± 0.18	...
...	2.4	4.3 ± 0.2	5.4	−0.15 ± 0.06	0.82 ± 0.15	...
48	981013	51099.61	C	4.99	10.8 ± 0.2	10.6	−0.18 ± 0.02	0.95 ± 0.01	...
...	10.0	3.6 ± 0.1	7.4	0.27 ± 0.06	0.85 ± 0.08	...
...	2.5	3.3 ± 0.2	7.6	−0.02 ± 0.04	0.82 ± 0.02	...
49	981014	51100.29	C	6.48	7.3 ± 0.2	12.0	−0.29 ± 0.03	0.90 ± 0.01	...
...	13.0	1.5 ± 0.1	13.0	0.34 ± 0.09	0.59 ± 0.08	...
...	3.2	3.5 ± 0.2	4.9	−0.15 ± 0.05	0.83 ± 0.04	...
50	981015	51101.61	C	6.85	6.4 ± 0.1	7.7	−0.28 ± 0.04	0.83 ± 0.02	141 ± 3
...	13.7	1.2 ± 0.1	11.1	0.10 ± 0.10	0.61 ± 0.11	...
...	3.4	3.1 ± 0.1	4.9	−0.25 ± 0.07	0.82 ± 0.04	...
51	981015	51101.94	C	6.77	7.5 ± 0.1	7.0	−0.34 ± 0.04	0.89 ± 0.01	145 ± 8
...	13.5	1.7 ± 0.1	7.7	0.30 ± 0.09	0.46 ± 0.05	...
...	3.4	4.5 ± 0.1	3.3	−0.31 ± 0.06	0.78 ± 0.03	...
52	981020	51106.95	B	5.46	3.5 ± 0.1	10.7	0.24 ± 0.04	0.99 ± 0.03	194 ± 15

Table 1—Continued

Obs #	Date (yyymmdd)	MJD ^a	Type	QPO ν^b (Hz)	Amplitude ^c (% rms)	Q ^d	Phase Lag ^e (radians)	Coherence ^f	HFQPO ^g (Hz)
...	10.9	1.5 ± 0.1	7.7	-0.54 ± 0.14	1.28 ± 0.34	...
...	2.7	0.7 ± 0.1	5.1	-0.53 ± 0.36	0.0 ± 1	...
53	981022	51108.08	B	5.4	4.0 ± 0.2^k	3.2	0.27 ± 0.02	0.98 ± 0.01	183 ± 3
...	10.9	2.2 ± 0.1	6.0	-0.39 ± 0.04	0.97 ± 0.05	...
...	2.7	1.5 ± 0.1	3.8	-0.35 ± 0.12	0.70 ± 0.22	...
54	981023	51109.74	B	4.94	3.8 ± 0.1	12.7	0.13 ± 0.03	0.99 ± 0.02	...
...	9.9	1.6 ± 0.1	8.3	-0.27 ± 0.15	0.99 ± 0.26	...
59	981029	51115.28	A	6.89	2.0 ± 0.1	2.8	-1.45 ± 0.51	0.1 ± 1	270 ± 6^1
...	16.6	0.53 ± 0.06	8.3	0.22 ± 0.59	0.0 ± 1	...
64	981109	51126.59	A?	4.88	1.5 ± 0.1	4.9	-1.78 ± 1.20	0.2 ± 1	284 ± 4^1
151	990302	51239.08	?	18.1	0.50 ± 0.03	18.9	-0.56 ± 0.19	0.9 ± 1	...
153	990304	51241.83	A	5.84	2.0 ± 0.1	5.8	-0.75 ± 0.11	1.3 ± 1	283 ± 2^1
154	990305	51242.51	A	5.62	1.3 ± 0.1	5.6	-1.34 ± 0.32	0.4 ± 1	283 ± 3^1
155	990307	51244.50	A?	8.45	1.3 ± 0.1	2.2	-0.76 ± 0.39	0.0 ± 1	...
156	990308	51245.35	B	6.38	3.3 ± 0.1^j	13.9	0.34 ± 0.03	0.96 ± 0.01	182 ± 2
...	12.2	1.3 ± 0.1^j	5.6	-0.44 ± 0.08	1.03 ± 0.13	...
...	3.1	1.5 ± 0.1^j	4.0	-0.63 ± 0.24	1.5 ± 1	...
157	990309	51246.41	A?	7.70	0.9 ± 0.1^j	4.3	-0.14 ± 0.35	1.0 ± 1	214 ± 7
158	990310	51247.98	B	6.15	3.4 ± 0.1^j	11.8	0.33 ± 0.03	0.97 ± 0.01	189 ± 6
...	3.1	1.6 ± 0.1	6.2	-0.49 ± 0.08	0.78 ± 0.08	...
159	990311	51248.09	B	5.89	3.5 ± 0.1	12.3	-0.50 ± 0.15	0.63 ± 0.11	...
...	12.3	1.3 ± 0.1	9.3	0.18 ± 0.04	1.00 ± 0.02	...
...	11.8	1.3 ± 0.1	8.5	-0.38 ± 0.14	1.06 ± 0.30	...
...	2.9	0.8 ± 0.1	6.1	-0.74 ± 0.43	0.6 ± 1	...
160	990312	51249.40	B	6.1	3.8 ± 0.1^j	9.4	0.34 ± 0.06	0.99 ± 0.03	185 ± 18
...	12.2	1.9 ± 0.1	5.7	-0.47 ± 0.14	1.41 ± 0.41	...
...	3.1	2.8 ± 0.1	5.3	-0.23 ± 0.17	0.74 ± 0.17	...
161	990313	51250.69	C	6.71	6.2 ± 0.1	9.4	-0.35 ± 0.04	0.89 ± 0.03	102 ± 3^1
...	13.4	1.5 ± 0.1	10.9	0.52 ± 0.15	0.51 ± 0.15	...
...	3.4	3.3 ± 0.2	5.0	-0.08 ± 0.07	0.72 ± 0.06	...
162	990316	51253.22	B	5.4	4.4 ± 0.1^j	5.0	0.27 ± 0.05	1.00 ± 0.03	...
...	10.7	2.2 ± 0.1^j	4.0	-0.47 ± 0.11	1.37 ± 0.34	...
...	2.9	2.1 ± 0.1^j	4.0	-0.18 ± 0.38	0.8 ± 1	...
163	990317	51254.09	B	5.95	3.0 ± 0.1	5.9	0.08 ± 0.08	0.62 ± 0.05	209 ± 6
...	3.0	1.8 ± 0.1	6.2	-0.47 ± 0.19	0.28 ± 0.05	...
164	990318	51255.09	A	10.1^l	8.0 ± 0.2	1.2	-0.90 ± 0.36	0.4 ± 1	281 ± 4^1
...	13.6	1.8 ± 0.1	2.1	0.02 ± 0.33	1.0 ± 1	...
166	990321	51258.30	A?	10.3^l	$6.9 \pm 0.2^{l,k}$	1.3	-0.43 ± 0.27	1.0 ± 1	275 ± 4^1
178	990402	51270.74	A?	7.1^l	$12.5 \pm 0.2^{l,k}$	~ 1	0.12 ± 0.19	1.7 ± 1	253 ± 9
179	990403	51271.41	A?	7.1^l	$12.5 \pm 0.2^{l,k}$	~ 1	-0.07 ± 0.22	1.0 ± 1	...

^aStart of observation, $MJD = JD - 2,400,000.5$.

^bQPO centroid frequency ; uncertainties are generally $< 5\%$ at the 95% confidence level.

^cThe QPO amplitude is the fractional rms fluctuation, calculated as the square root of the integrated power in the QPO feature and expressed as a fraction of the mean count rate. Errors are 1σ , with a lower limit of 0.1% for systematic uncertainty in the continuum model, except for especially narrow QPOs ($Q > 10$).

^d $Q = \text{QPO Frequency}/\text{FWHM}$

^ePhase lag between 2–13 keV and 13–30 keV bands at the QPO center. A positive value corresponds to a hard lag. Errors are 1σ .

^fCoherence between the two energy bands at the QPO center. Errors are 1σ .

^gHigh-frequency QPOs detected with 4σ level of confidence, nominally over the full energy range of the PCA instrument.

^hSpecial cases (noted in col. 1). soft band: 2–11.3 keV; hard band 11.3–18.3 keV.

ⁱSpecial cases (noted in col. 1). soft band: 2–6.5 keV; hard band: 6.5–30 keV.

Table 2. Summary of QPO Types

Property	Type A ^a	Type B	Type C
Frequency (Hz)	~ 6	5–6	0.1–10
Amplitude (%rms)	3–4	~ 4	3–16
Q ($\nu/FWHM$)	~ 2 –4	~ 4	$\gtrsim 10$
Phase Lag (rad.)	–0.6 to –1.4	0 to 0.4	0.05 to –0.4
Sub-Harmonic	...	soft	soft
1st Harmonic	soft	soft	hard
Coherence	< 0.5	~ 1	~ 0.9
HFQPO ^b	4/4	6/9	5/51

^aThis column excludes the 6 “A?” type QPOs, which have broad profiles but statistically uncertain measurements of the coherence function.

^bIn addition to these, HFQPOs are seen in one peculiar type and in 4 of 6 “A?” type of LFQPO.

Fig. 1.— Characteristic power spectrum (top), phase lag spectrum (middle), and coherence function (bottom) for Type A QPOs (left panels) and Type B QPOs (right panels). The phase lag and coherence are computed between the 2–13 keV and 13–30 keV bands, with a positive phase lag representing a hard lag.

Fig. 2.— Characteristic power spectrum (top), phase lag spectrum (middle), and coherence function (bottom) for Type C QPOs (left panels) and Type C' QPOs (right panels).

Fig. 3.— Characteristic power spectrum (top), phase lag spectrum (middle), and coherence function (bottom) for two anomalous QPOs which do not resemble types A, B, or C (see text).

Fig. 4.— Phase lag in the fundamental feature vs. frequency (left panel) and integrated rms amplitude (right panel). The plotting symbols distinguish the QPO type: Types A and A' – open triangles, Type B – open squares, Type C – filled circles, Type C' – open circles, and the anomalous – 'x'.

Fig. 5.— QPO properties (fundamental feature) versus the color temperature (keV) of the accretion disk (left panels), the unabsorbed disk flux at 2–20 keV (center panels) and the bolometric disk flux (right panels). The fluxes are in units of 10^{-7} ergs cm^{-2} s^{-1} , and the plotting symbols are the same as in Fig. 4.

Fig. 6.— QPO phase lag (fundamental feature) versus the fraction of the unabsorbed, total flux attributed to the accretion disk. In the left panel, the integration of each spectral component is limited to the range 2–20 keV. In the right panel we consider the entire disk-blackbody spectrum, and we integrate the spectrum of the power-law component over the range 1–30 keV. The latter is subject to increased systematic uncertainty due to the extrapolation of the spectrum well beyond the sensitivity band of the PCA instrument. The plotting symbols are the same as in Fig. 4.

Fig. 7.— The frequencies of HFQPOs in XTE—J1550–564 versus the LFQPO fundamental (top panel) and the fundamental's Q value (bottom panel). The plotting symbols are the same as in Fig. 4. The LFQPO type (but not the actual frequency) is correlated with the frequency of the HFQPOs, while the fundamental's Q value decreases as the HFQPOs progress toward narrow profiles and hard spectra when seen at 284 Hz.

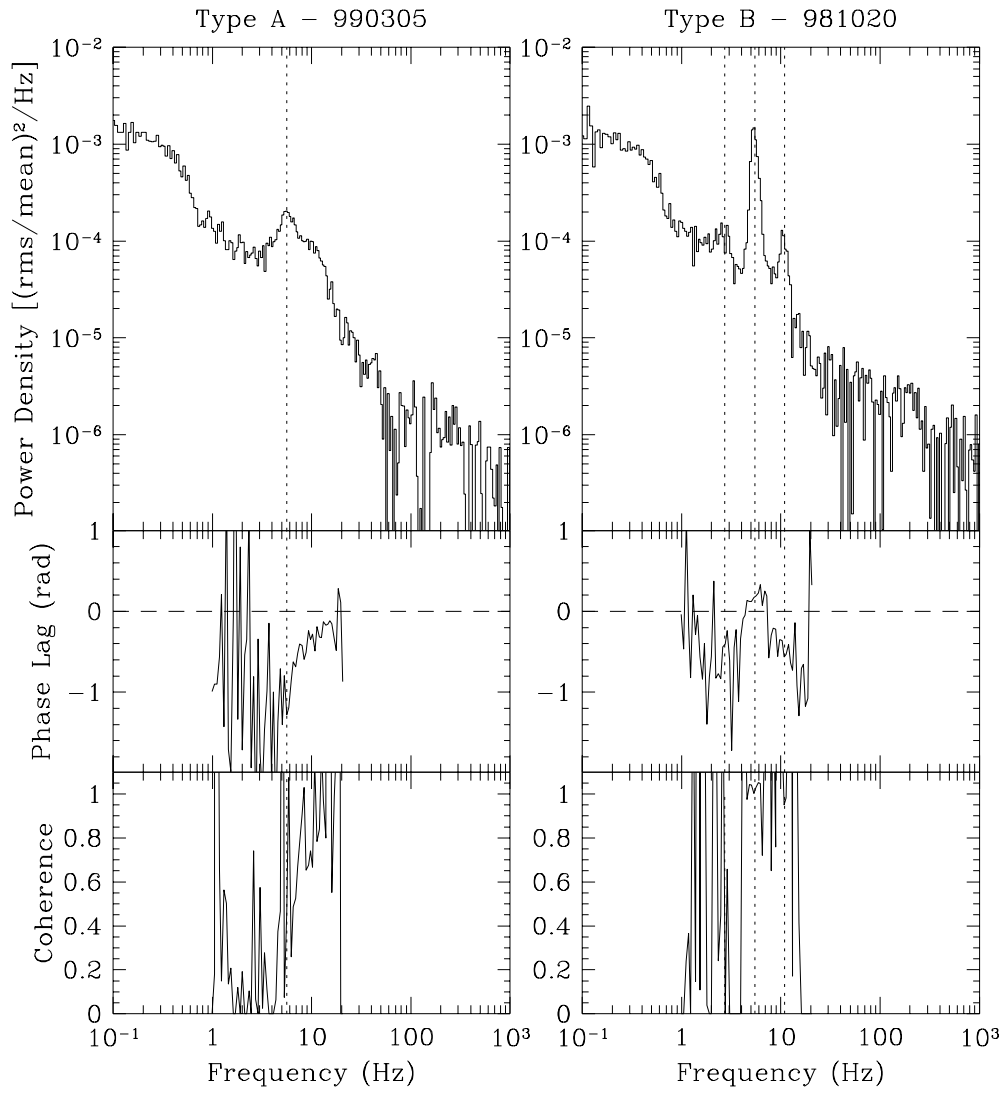


Fig. 1.—

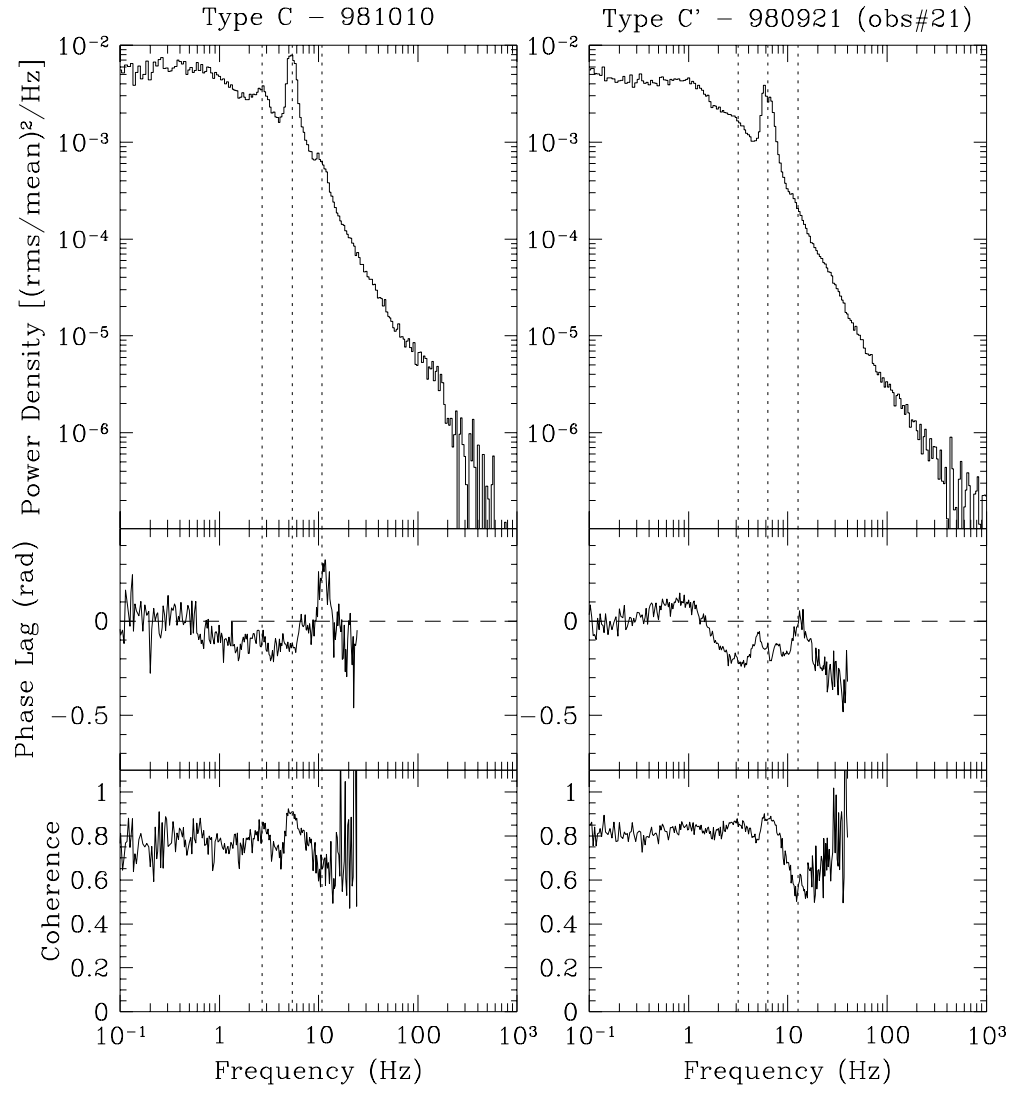


Fig. 2.—

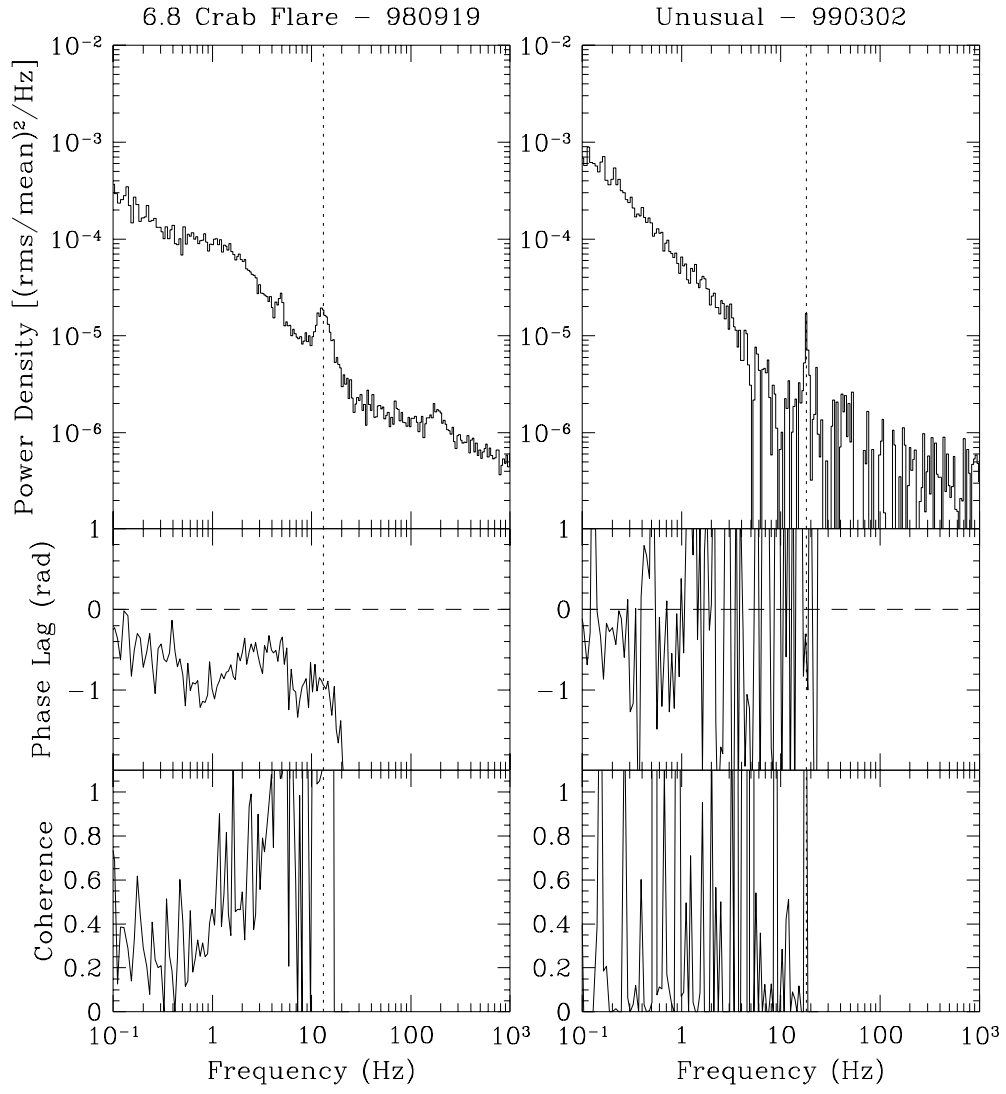


Fig. 3.—

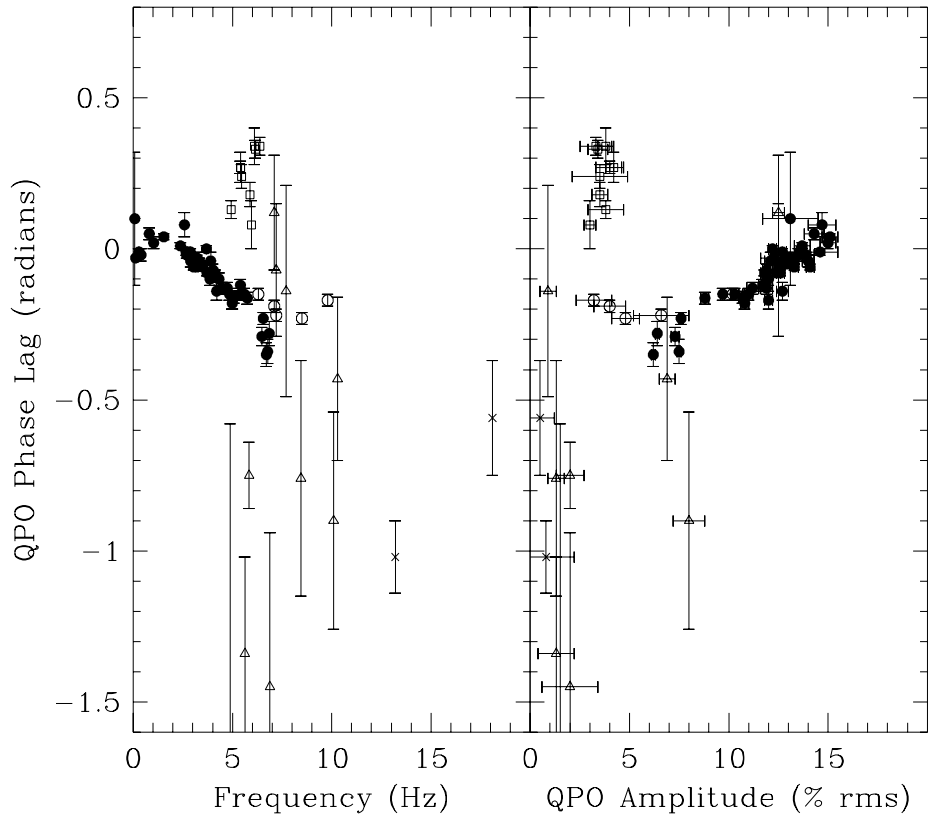


Fig. 4.—

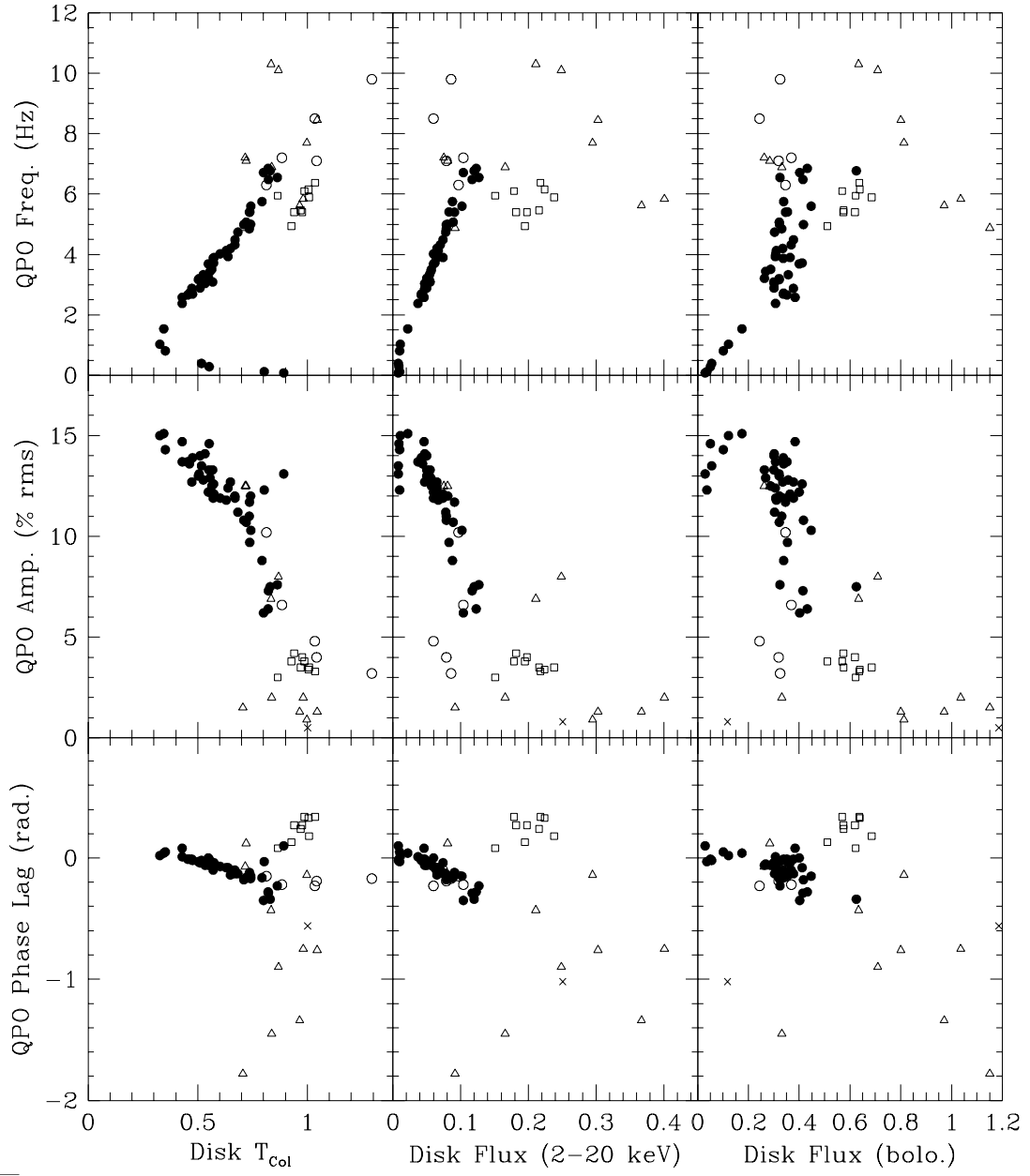


Fig. 5.—

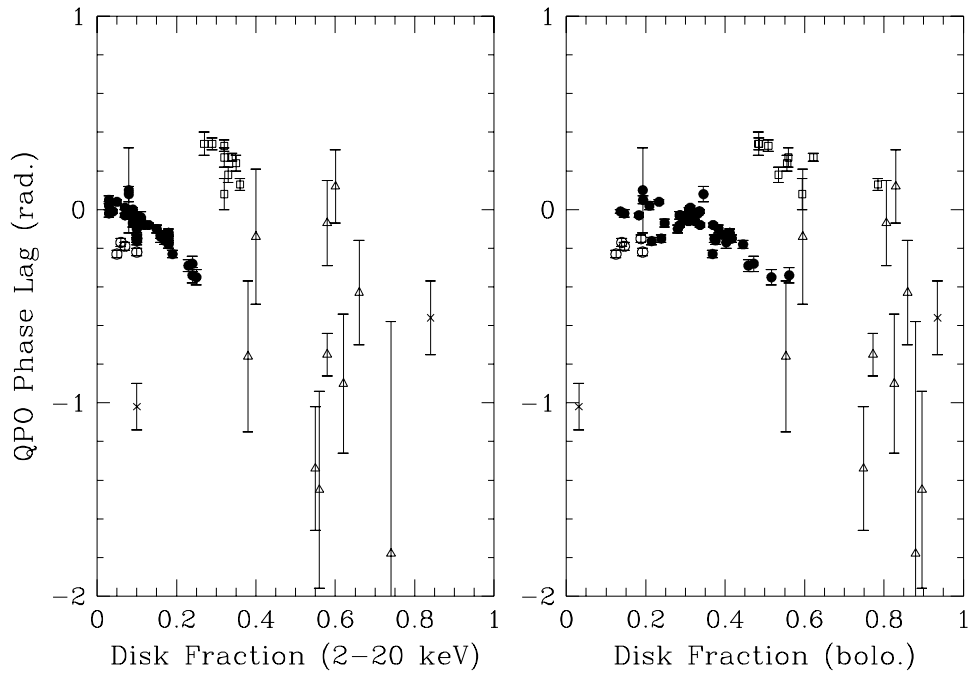


Fig. 6.—

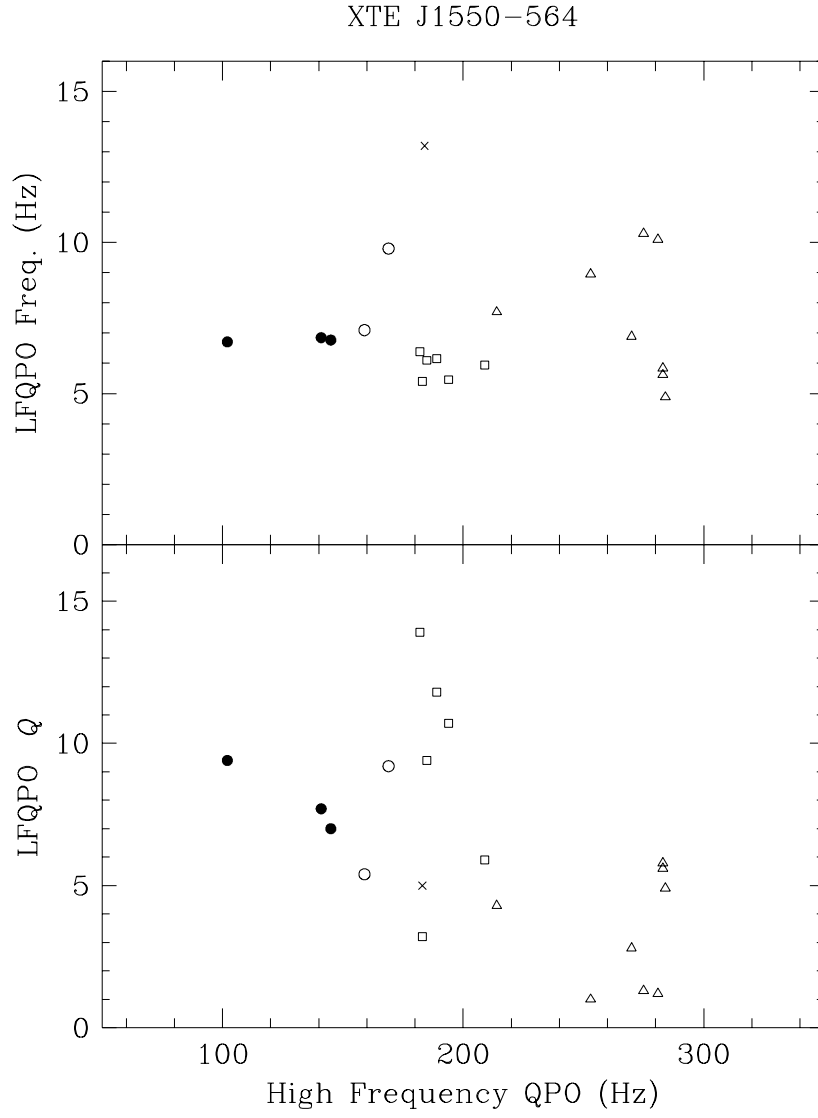


Fig. 7.—